

Lattice Boltzmann Modeling of Advection-Diffusion-Reaction Equations: Pattern Formation Under Uniform Differential Advection

S. G. Ayodele^{1,*}, D. Raabe¹ and F. Varnik^{1,2}

¹ *Max-Planck Institut für Eisenforschung, Max-Planck Straße 1, 40237, Düsseldorf, Germany.*

² *Interdisciplinary Center for Advanced Materials Simulation, Ruhr University Bochum, Stiepelstraße 129, 44780 Bochum, Germany.*

Received 31 October 2011; Accepted (in revised version) 27 January 2012

Available online 29 August 2012

Abstract. A lattice Boltzmann model for the study of advection-diffusion-reaction (ADR) problems is proposed. Via multiscale expansion analysis, we derive from the LB model the resulting macroscopic equations. It is shown that a linear equilibrium distribution is sufficient to produce ADR equations within error terms of the order of the Mach number squared. Furthermore, we study spatially varying structures arising from the interaction of advective transport with a cubic autocatalytic reaction-diffusion process under an imposed uniform flow. While advecting all the present species leads to trivial translation of the Turing patterns, differential advection leads to flow induced instability characterized with traveling stripes with a velocity dependent wave vector parallel to the flow direction. Predictions from a linear stability analysis of the model equations are found to be in line with these observations.

AMS subject classifications: 76R05, 76R50, 92C15, 80A32

Key words: Advective transport, differential advection, Turing patterns, linear stability, lattice Boltzmann.

1 Introduction

Spatially and/or temporally varying structures have been observed in a variety of physical [1, 2], chemical [3–5] and biological [6–11] systems operating far from equilibrium. In chemical and biological systems for instance, the macroscopic reaction-diffusion (RD) equations have been proposed as models for morphogenesis [12], pattern formation [6, 7] and self-organization [13, 14]. This class of equations usually includes the following two

*Corresponding author. *Email addresses:* s.ayodele@mpie.de (S. G. Ayodele), d.raabe@mpie.de (D. Raabe), fathollah.varnik@rub.de (F. Varnik)

features: (i) a nonlinear reaction between chemical species describing local production or consumption of the species and (ii) the diffusive transport of these species due to density gradients. The properties of structures that arise from this class of systems are determined by the intrinsic transport parameters of the system such as the diffusion coefficient and reaction constants. However, the presence of an external influence such as advection may lead to qualitative changes in the system's behavior and to the emergence of new non-equilibrium structures. This is very important in the experimental investigations of the diffusive chemical instability in gel reactors where the perturbative effect of the feeding flows is not fully suppressed or in tubular reactors where spatiotemporal behaviors might also be of interest. Attempts to understand the role played by advection in spatio-temporal organization of RD systems have led to the discovery of the flow distributed structures (FDS) or flow distributed oscillations (FDO). In this case excitable RD systems with fixed or periodically forced inflow boundary, are known to develop stationary [15, 16] and traveling waves [17, 18] depending on the boundary-forcing frequency. Patterns of these type are known to occur even when the Turing instability condition of unequal diffusion coefficient is not satisfied.

A closely related problem to the boundary forced structures which have received less study in 2D is the interactions between advective fields and a pre-existing sharp chemical gradients produced by reaction-diffusion processes. This means the interaction of already existing instabilities with the instability caused by advection. This interaction can give rise to complex patterns in both chemical and biological systems [19, 20]. In this work we consider the interaction of a uniform flow field with the Turing instability. As a prominent example of an autocatalytic reaction-diffusion pattern forming system we choose the Gray-Scott model [23]. This model has some generic features which can make it adaptable to study some realistic situations such as vegetative patterns, combustion and cell division [21, 22]. We propose a Lattice Boltzmann (LB) method for solving the ADR equations arising from the interaction of the advective fields with the Turing patterns. The LB simulation of the ADR equations shows that while advecting all the species leads to trivial translation of the Turing patterns, differential advection of the species leads to an additional flow induced instability characterized by traveling stripes with a velocity dependent wave vector parallel to the flow direction. These observations are in line with the predictions from linear stability analysis carried out on the model equations. The article is organized as follows. In the next section, we present the model equations. In Section 3 we address the framework adopted for the Lattice Boltzmann modeling of the model equations. The results obtained from the linear stability analysis and numerical simulations are discussed in Section 4. At the end of the same section, we conclude the discussion with a summary of our results.

2 The model equations

In this section we present the governing equations for the Gray-Scott advection-diffusion-reaction (ADR) model. The original Gray-Scott reaction-diffusion model describes the ki-

netics of a simple autocatalytic reaction in an un-stirred homogeneous flow reactor [23]. The reactor is confined in a narrow space between two porous walls in contact with a reservoir. Substance A whose density is kept fixed at A_0 in the reservoir outside of the reactor is supplied through the walls into the reactor with the volumetric flow rate per unit volume k_f . Inside the reactor, A undergoes an autocatalytic reaction with an intermediate species B at a rate k_1 . The species B then undergoes a decay reaction to an inert product C at a rate k_2 . The product C and excess reactants A and B are then removed from the reactor at the same flow rate per unit volume k_f . The basic reaction steps are summarized as follows



The reaction in Eq. (2.1a) is the cubic autocatalytic reaction in which two molecules of species B produce three molecules of B through interaction with the species A. The presence of B stimulates further production of itself, while the presence of A controls the production of B. Substance A is sometimes called the inhibitor and B the activator. By constantly feeding the reactor with a uniform flow of species A while at the same time removing the product and excess reactants, far from equilibrium conditions can be maintained. Note that inside the reactor the two species A and B are assumed to interact only through the non-linear autocatalytic reaction in Eq. (2.1a). In particular, interaction terms due to cross diffusion between the species are neglected. This assumption is physically justified as pattern forming systems often occur in the form of dilute solutions. Following this assumption, the equations of chemical kinetics which describe the above situations and include the spatio-temporal variations of the concentrations of A and B in the reactor take the following form:

$$\frac{\partial A}{\partial t} = k_f(A_0 - A) - k_1 B^2 A + D_A \nabla^2 A, \quad (2.2a)$$

$$\frac{\partial B}{\partial t} = -(k_f + k_2) B + k_1 B^2 A + D_B \nabla^2 B, \quad (2.2b)$$

where A and B are the density of species A and B respectively, A_0 is the density of A in the reservoir, while D_A and D_B are the diffusion coefficients of species A and B respectively. To account for the effect of an imposed flow, one simply adds a term due to advection to the Gray-Scott reaction-diffusion Eqs. (2.2a) and (2.2b). However, note that the two dimensional reaction-diffusion model described above contains a constant feed flow term ($k_f A_0$) perpendicular to the reaction surface. This feed flow term constantly replenishes species A on the reaction surface and thus species A is therefore sometimes referred to as the substrate. But in a variety of technical settings or Tubular flow reactors the external field that drives the system enters from one end and the idea of modeling advection by driving species A and B with flow velocity u parallel to the surface is physically justified. In the case of the velocity field considered here, an incompressible flow

with divergence free velocity field, the advection-diffusion-reaction (ADR) describing the transport of species A and B can then be written as:

$$\frac{\partial A}{\partial t} = k_f(A_0 - A) - k_1 B^2 A + D_A \nabla^2 A - \mathbf{u} \cdot \nabla A, \quad (2.3a)$$

$$\frac{\partial B}{\partial t} = -(k_f + k_2) B + k_1 B^2 A + D_B \nabla^2 B - \delta \mathbf{u} \cdot \nabla B, \quad (2.3b)$$

where the parameter δ is the ratio of the advective rates of the two species or the differential advection parameter. The absence and presence of differential advection is modeled with the parameter $\delta = 1$ and $\delta \neq 1$ respectively. Here we focus on the situations with $\delta = 1$ and $\delta = 0$.

In order to proceed with the analysis of Eq. (2.3), it is important to reduce the number of parameters and introduce variables in the form of time and length scales that represent the physical processes acting in the system. We therefore introduce concentration scales (A_0, B_0) , time scales $(\tau_A = 1/k_f, \tau_B = 1/(k_f + k_2))$, length scales $(l_A = (D_A \tau_A)^{1/2}, l_B = (D_B \tau_B)^{1/2})$ and velocity scale $u_A = l_A / \tau_A$ such that:

$$\tilde{t} = \frac{t}{\tau_A}, \quad \tilde{A} = \frac{A}{A_0}, \quad \tilde{B} = \frac{B}{B_0}, \quad (\tilde{x}, \tilde{y}) = \frac{1}{l_A}(x, y), \quad \tilde{u} = \frac{u}{u_A}, \quad B_0 = (k_f / k_1)^{1/2}. \quad (2.4)$$

Using the above relations in Eq. (2.3) we arrive at the non-dimensional equations as:

$$\frac{\partial \tilde{A}}{\partial \tilde{t}} = (1 - \tilde{A}) - \tilde{B}^2 \tilde{A} + \tilde{\nabla}^2 \tilde{A} - \tilde{\mathbf{u}} \cdot \tilde{\nabla} \tilde{A}, \quad (2.5a)$$

$$\frac{1}{\tau} \frac{\partial \tilde{B}}{\partial \tilde{t}} = -\tilde{B} + \eta \tilde{B}^2 \tilde{A} + \frac{1}{\varepsilon^2} \tilde{\nabla}^2 \tilde{B} - \frac{\delta}{\tau} \tilde{\mathbf{u}} \cdot \tilde{\nabla} \tilde{B}, \quad (2.5b)$$

where the parameter

$$\eta = \frac{A_0(k_1 k_f)^{1/2}}{(k_f + k_2)}, \quad \tau = \tau_A / \tau_B, \quad \varepsilon = l_A / l_B = \sqrt{\tau_A D_A / \tau_B D_B}. \quad (2.6)$$

Eqs. (2.5a) and (2.5b) have three simple equilibrium solutions which correspond to a spatially homogeneous situation with no fluid flow ($\mathbf{u} = 0$). The first solution is the trivial homogeneous solution $\tilde{B}_e = 0, \tilde{A}_e = 1$. This state exist for all system parameters. The other two solutions exist provided that $\eta > 2$. These are given by:

$$\tilde{A}_e^\pm = \frac{\eta \pm \sqrt{\eta^2 - 4}}{2\eta}, \quad \tilde{B}_e^\pm = \frac{\eta \mp \sqrt{\eta^2 - 4}}{2}. \quad (2.7)$$

In equilibrium, the system can be found in any of these states and any external activation or perturbation added to these states would either grow far from the equilibrium state to a patterned state or decays back towards the equilibrium. The nature of the time evolution from equilibrium depends on the systems transport parameters.

3 Lattice Boltzmann modeling

Lattice Boltzmann schemes have been used to study the advection, diffusion and reaction of a scalar field in reactive chemical transport processes [24–26]. In this work we introduce the framework adopted for modeling advection-diffusion-reaction in domains with no-flux boundary condition. In general, the lattice Boltzmann method [27–30] can be regarded as a mesoscopic particle based numerical approach allowing to solve fluid dynamical equations in a certain approximation, which (within, e.g. the so called diffusive scaling, i.e. by choosing $\Delta t = \Delta x^2$) becomes exact as the grid resolution is progressively increased. The density of the fluid at each lattice site is accounted for by a one particle probability distribution $f_i(\mathbf{x}, t)$, where \mathbf{x} is the lattice site, t is the time and the subscript i represents one of the finite velocity vectors \mathbf{e}_i at each lattice node. The number and direction of the velocities are chosen such that the resulting lattice is symmetric so as to easily reproduce the isotropy of the fluid [31]. During each time step, particles stream along each velocity vector \mathbf{e}_i to a neighboring lattice site and collide locally, conserving mass and momentum in the process.

In order to use this method to simulate the ADR equations, we introduce a multi-species distribution function $f_{i,j}$ where the subscript j runs over the number of species $j = 1, \dots, n_s$. As stated above, here, we assume that the diffusion of a given species does not depend on the concentration of other species. In other words, the species in our model do not interact among each other, except through the chemical reaction term. This assumption is physically justified since many pattern forming systems are studied in the form of dilute solutions. At higher concentrations, however, the mutual interactions of different species shall be taken into account [32, 33]. The species field $f_{i,j}$ is advected with the imposed flow velocity \mathbf{u} and does not have any effect on the velocity field (passive tracer limit). The chemical reaction is modeled by including a source term, R_j , in the collision step. The LB-BGK equation governing propagation, collision of the density (concentration) distribution of the passive tracers is given as:

$$f_{i,j}(\mathbf{x} + \mathbf{e}_i, t + 1) - f_{i,j}(\mathbf{x}, t) = \frac{f_{i,j}^{\text{eq}}(\mathbf{x}, t) - f_{i,j}(\mathbf{x}, t)}{\tau_j} + w_i R_j, \quad (3.1)$$

where τ_s is the relaxation time for species s and $f_{i,j}^{\text{eq}}$ is the equilibrium distribution function expanded up to the linear order in velocity as $f_{i,j}^{\text{eq}}(\mathbf{x}, t) = w_i \rho_j [1 + (\mathbf{e}_i \cdot \mathbf{u}) / c_s^2]$. As will be shown below, the expansion to linear order is sufficient to recover the ADR equation considered in this study. In the expression for the equilibrium distribution, c_s is the sound speed on the lattice and w_i is a set of weights normalized to unity. The weights w_i in the equilibrium distribution depend on the number of velocities used for the lattice. In this work, we have used the two dimensional nine velocity (D2Q9) model, with the sound speed c_s given as $c_s^2 = c^2 / 3$, where $c = \Delta x / \Delta t$ is the lattice speeds. The lattice weights and

number of velocities for the D2Q9 is given as

$$w_i = \begin{cases} 4/9, & \mathbf{e}_i = (0, 0), i=0; \\ 1/9, & \mathbf{e}_i = (\pm 1, 0), (0, \pm 1), i=1, \dots, 4; \\ 1/36, & \mathbf{e}_i = (\pm 1, \pm 1), i=5, \dots, 8. \end{cases} \quad (3.2)$$

The source term R_j represents the rate of change of density of the species, j , with regard to reaction kinetics. The exact form of the relation between the reaction rate R_j and the density (concentration) of each species depends on the type of reaction being modeled. In this work, for species A, the reaction term is taken as $R_1 = k_f(A_0 - A) - k_1 B^2 A$ and for species B, $R_2 = -(k_f + k_2)B + k_1 B^2 A$. The density of the species j , is computed by taking the zeroth moment of the distribution function, i.e. $A = \sum_{i=0}^N f_{i,1}$ and $B = \sum_{i=0}^N f_{i,2}$, where $N=8$ in the present D2Q9 model. The corresponding macroscopic ADR equation can be recovered from the LB Eq. (3.1) by performing a multiscale Chapman-Enskog expansion. We present a brief outline of the derivation and discuss the contribution of the error terms to the ADR equations in the following section.

3.1 Chapman-Enskog procedure for the derivation of ADR equation

In this section, we derive the macroscopic ADR equation from the lattice Boltzmann equation;

$$f_{i,j}(\mathbf{x} + \mathbf{e}_i \Delta t, \Delta t + t) - f_{i,j}(\mathbf{x}, t) = \frac{f_{i,j}^{\text{eq}}(\mathbf{x}, t) - f_{i,j}(\mathbf{x}, t)}{\tau_j} + \Delta t w_i R_j. \quad (3.3)$$

By performing a Taylor series expansion of the left hand side of Eq. (3.3), a partial differential term can be written in place of the finite difference term as

$$\sum_{n=1}^{\infty} \frac{\Delta t^n}{n!} (\partial_t + e_{i\alpha} \partial_{x_\alpha})^n f_{i,j}(\mathbf{x}, t) = \frac{f_{i,j}^{\text{eq}}(\mathbf{x}, t) - f_{i,j}(\mathbf{x}, t)}{\tau_j} + \Delta t w_i R_j. \quad (3.4)$$

The distribution functions, time derivative, spatial derivative and the reaction term R_j are expanded in terms of a smallness parameter, ϵ , as [34,35]

$$f_{i,j} = f_{i,j}^{(0)} + \epsilon f_{i,j}^{(1)} + \epsilon^2 f_{i,j}^{(2)} + \epsilon^3 f_{i,j}^{(3)} + \mathcal{O}(\epsilon^4), \quad (3.5a)$$

$$\partial_t = \epsilon \partial_t^{(1)} + \epsilon^2 \partial_t^{(2)}, \quad (3.5b)$$

$$\partial_{x_\alpha} = \epsilon \partial_{x_\alpha}^{(1)}, \quad (3.5c)$$

$$R_j = \epsilon^2 R_j^{(2)} + \epsilon^3 R_j^{(3)} + \mathcal{O}(\epsilon^4). \quad (3.5d)$$

A natural interpretation of the parameter ϵ is the so called Knudsen number, the ratio of the fluids mean free path to a characteristic dimension for variations of the macroscopic

velocity field. Inserting Eqs. (3.5a), (3.5b), (3.5c) and (3.5d) in Eq. (3.4), one obtains

$$\begin{aligned} & \left[\Delta t (\epsilon \partial_t^{(1)} + \epsilon^2 \partial_t^{(2)} + \epsilon e_{i\alpha} \partial_{x_\alpha}^{(1)}) + \frac{\Delta t^2}{2} (\epsilon^2 \partial_t^{(1)} \partial_t^{(1)} + 2\epsilon^2 e_{i\alpha} \partial_t^{(1)} \partial_{x_\alpha}^{(1)} + \epsilon^2 e_{i\alpha} e_{i\beta} \partial_{x_\alpha}^{(1)} \partial_{x_\beta}^{(1)} \right. \\ & \quad \left. + 2\epsilon^3 e_{i\alpha} \partial_t^{(2)} \partial_{x_\alpha}^{(1)} + 2\epsilon^3 \partial_t^{(2)} \partial_t^{(1)} + 2\epsilon^4 \partial_t^{(2)} \partial_t^{(2)} \right] (f_{i,j}^{(0)} + \epsilon f_{i,j}^{(1)} + \epsilon^2 f_{i,j}^{(2)} + \mathcal{O}(\epsilon^3)) \\ &= \frac{1}{\tau_j} \left(f_{i,j}^{\text{eq}}(\mathbf{x}, t) - (f_{i,j}^{(0)} + \epsilon f_{i,j}^{(1)} + \epsilon^2 f_{i,j}^{(2)} + \epsilon^3 f_{i,j}^{(3)} + \mathcal{O}(\epsilon^4)) \right) \\ & \quad + \Delta t w_i (\epsilon R_j^{(1)} + \epsilon^2 R_j^{(2)} + \epsilon^3 R_j^{(3)} + \mathcal{O}(\epsilon^4)). \end{aligned} \tag{3.6}$$

Grouping terms of the same order in ϵ yields the following successive approximations

$$\mathcal{O}(\epsilon^0): \quad f_{i,j}^{(0)} = f_{i,j}^{\text{eq}}, \tag{3.7}$$

$$\mathcal{O}(\epsilon^1): \quad \Delta t \left(\partial_t^{(1)} + e_{i\alpha} \partial_{x_\alpha}^{(1)} \right) f_{i,j}^{(0)} = -\frac{1}{\tau_j} f_{i,j}^{(1)}, \tag{3.8}$$

$$\begin{aligned} \mathcal{O}(\epsilon^2): \quad & \Delta t \left(\partial_t^{(2)} f_{i,j}^{(0)} + \left(\partial_t^{(1)} + e_{i\alpha} \partial_{x_\alpha}^{(1)} \right) f_{i,j}^{(1)} \right) + \frac{\Delta t^2}{2} \left(\partial_t^{(1)2} + 2e_{i\alpha} \partial_t^{(1)} \partial_{x_\alpha}^{(1)} + e_{i\alpha} e_{i\beta} \partial_{x_\alpha}^{(1)} \partial_{x_\beta}^{(1)} \right) f_{i,j}^{(0)} \\ &= -\frac{1}{\tau_j} f_{i,j}^{(2)} + \Delta t w_i R_j^{(2)}, \end{aligned} \tag{3.9}$$

$$\begin{aligned} \mathcal{O}(\epsilon^3): \quad & \Delta t \left(\partial_t^{(3)} f_{i,j}^{(0)} + \partial_t^{(2)} f_{i,j}^{(1)} + \left(\partial_t^{(1)} + e_{i\alpha} \partial_{x_\alpha}^{(1)} \right) f_{i,j}^{(2)} \right) d + \frac{\Delta t^2}{2} \left(\partial_t^{(1)3} + 2e_{i\alpha} \partial_t^{(1)} \partial_{x_\alpha}^{(1)} \right. \\ & \quad \left. + e_{i\alpha} e_{i\beta} \partial_{x_\alpha}^{(1)} \partial_{x_\beta}^{(1)} \right) f_{i,j}^{(1)} + \Delta t^2 \partial_t^{(2)} \left(\partial_t^{(1)} + e_{i\alpha} \partial_{x_\alpha}^{(1)} \right) f_{i,j}^{(0)} + \frac{\Delta t^3}{6} \left(\partial_t^{(1)} + e_{i\alpha} \partial_{x_\alpha}^{(1)} \right)^3 f_{i,j}^{(0)} \\ &= -\frac{1}{\tau_j} f_{i,j}^{(3)} + \Delta t w_i R_j^{(3)}. \end{aligned} \tag{3.10}$$

Putting the expression for $f_{i,j}^{(1)}$ from Eq. (3.8) into Eq. (3.9) yields

$$\frac{1}{\tau_j} f_{i,j}^{(2)} = -\Delta t \partial_t^{(2)} f_{i,j}^{(0)} + \Delta t^2 \left(\tau_j - \frac{1}{2} \right) \left(\partial_t^{(1)} + e_{i\alpha} \partial_{x_\alpha}^{(1)} \right)^2 f_{i,j}^{(0)} + \Delta t w_i R_j^{(2)}. \tag{3.11}$$

In Eq. (3.10), we insert the expression for $f_{i,j}^{(1)}$ and $f_{i,j}^{(2)}$ from Eqs. (3.8) and (3.9) and obtain

$$\begin{aligned} \frac{1}{\tau_j} f_{i,j}^{(3)} &= -\Delta t \partial_t^{(3)} f_{i,j}^{(0)} + \Delta t^2 (2\tau_j - 1) \left(\partial_t^{(1)} + e_{i\alpha} \partial_{x_\alpha}^{(1)} \right) \partial_t^{(2)} f_{i,j}^{(0)} - \Delta t^3 \left(\tau_j^2 - \tau_j + \frac{1}{6} \right) \left(\partial_t^{(1)} \right. \\ & \quad \left. + e_{i\alpha} \partial_{x_\alpha}^{(1)} \right)^3 f_{i,j}^{(0)} - \tau_s \Delta t^2 \left(\partial_t^{(1)} + e_{i\alpha} \partial_{x_\alpha}^{(1)} \right) w_i R_j^{(2)} + \Delta t w_i R_j^{(3)}. \end{aligned} \tag{3.12}$$

Next, we take the moments of the distribution functions in Eqs. (3.8), (3.11) and (3.12). Note that, since mass is conserved upon collision, only the equilibrium distribution function contributes to the local values of the mass. In other words, $\sum_{i=0}^N f_{i,j}^{(k)} = 0$, for all higher

order corrections, $k > 0$, and all species, j . For the purpose of comparison, we consider here two different equilibrium distribution, the linearized form

$$f_{i,j}^{(0)} = \rho_j w_i (1 + e_{i\alpha} u_\alpha / c_s^2), \quad (3.13)$$

and the quadratic form

$$f_{i,j}^{(0)} = \rho_j w_i \left(1 + \frac{1}{c_s^2} e_{i\alpha} u_\alpha + \frac{u_\alpha u_\beta}{2c_s^2} \left(\frac{e_{i\alpha} e_{i\beta}}{c_s^2} - \delta_{\alpha\beta} \right) \right). \quad (3.14)$$

Starting with the linear equilibrium distribution, the zeroth, first and second moments are given as:

$$\sum_i f_{i,j}^{(0)} = \rho_j, \quad \sum_i f_{i,j}^{(0)} e_{i\alpha} = \rho_j u_\alpha, \quad \sum_i f_{i,j}^{(0)} e_{i\alpha} e_{i\beta} = \rho_j c_s^2. \quad (3.15)$$

Taking \sum_i of Eq. (3.8) and using Eq. (3.15), yields

$$\partial_t^{(1)} \rho_j + \partial_{x_\alpha}^{(1)} (\rho_j u_\alpha) = 0. \quad (3.16)$$

Again, taking \sum_i of Eq. (3.11) and using Eqs. (3.15) and (3.16) yields

$$\partial_t^{(2)} \rho_j = \Delta t \left(\tau_j - \frac{1}{2} \right) \left(\partial_t^{(1)} \partial_{x_\alpha}^{(1)} \rho_j u_\alpha + c_s^2 \partial_{x_\alpha}^{(1)} \partial_{x_\alpha}^{(1)} \rho_j \right) + \Delta t R_j^{(2)}. \quad (3.17)$$

Adding together Eq. (3.16) $\times \epsilon$ and Eq. (3.17) $\times \epsilon^2$ leads to

$$\partial_t \rho_j + \partial_{x_\alpha} (\rho_j u_\alpha) = \Delta t \left(\tau_j - \frac{1}{2} \right) (c_s^2 \partial_{x_\alpha}^2 \rho_j + R_j + \partial_t \partial_{x_\alpha} \rho_j u_\alpha). \quad (3.18)$$

Comparing Eq. (3.17) with the ADR equations, the diffusion coefficient can be taken as $D_s = c_s^2 \Delta t (\tau_j - 1/2)$ and we can rewrite Eq. (3.18) as

$$\partial_t \rho_j + \partial_{x_\alpha} (\rho_j u_\alpha) = D_j \partial_{x_\alpha}^2 \rho_j + R_j + \frac{D_j}{c_s^2} \partial_t \partial_{x_\alpha} \rho_j u_\alpha, \quad (3.19)$$

with an error term $E_1 = D_j / c_s^2 \partial_t \partial_{x_\alpha} \rho_j u_\alpha$.

Alternatively, using the quadratic equilibrium distribution in Eq. (3.17) and following the above procedure, one obtains

$$\partial_t \rho_j + \partial_{x_\alpha} (\rho_j u_\alpha) = D_j \partial_{x_\alpha}^2 \rho_j + R_j + \frac{D_j}{c_s^2} \left(\partial_t \partial_{x_\alpha} (\rho_j u_\alpha) + \partial_{x_\alpha} \partial_{x_\beta} (\rho_j u_\alpha u_\beta) \right), \quad (3.20)$$

where the error term is now identified to be $E_2 = D_j / c_s^2 (\partial_t \partial_{x_\alpha} (\rho_j u_\alpha) + \partial_{x_\alpha} \partial_{x_\beta} (\rho_j u_\alpha u_\beta))$.

We remark that, in the both cases of the equilibrium distributions considered, the ADR equations are recovered at $\mathcal{O}(\epsilon^2)$. The contribution to the error term from the reaction rate kinetics only enters the equations at $\mathcal{O}(\epsilon^3)$. Indeed, after a little bit of algebra, one finds that a term of $\mathcal{O}(u^2 / c_s^2)$, due to spurious diffusion, is always present whether or not terms of $\mathcal{O}(u^2)$ are included in the local equilibrium distribution [36,37]. This term can however be neglected provided that $u^2 / c_s^2 \ll 1$ [37]. This condition is easily satisfied in our simulations.

4 Results and discussion

In this section, we discuss the results obtained from the numerical simulation of the Turing patterns under the imposed flow. We first begin with the linear stability analysis of the ADR equations, and then test some of the predictions of the linear stability analysis by performing numerical simulations.

4.1 Linear stability of the advection-diffusion-reaction equations

The dimensionless ADR equation is written as

$$\frac{\partial \tilde{A}}{\partial \tilde{t}} = (1 - \tilde{A}) - \tilde{B}^2 \tilde{A} + \tilde{\nabla}^2 \tilde{A} - \tilde{u} \cdot \tilde{\nabla} \tilde{A}, \quad (4.1a)$$

$$\frac{1}{\tau} \frac{\partial \tilde{B}}{\partial \tilde{t}} = -\tilde{B} + \eta \tilde{B}^2 \tilde{A} + \frac{1}{\varepsilon^2} \tilde{\nabla}^2 \tilde{B} - \frac{\delta}{\tau} \tilde{u} \cdot \tilde{\nabla} \tilde{B}. \quad (4.1b)$$

To determine the conditions for pattern formation, we add to the equilibrium states in Eq. (2.7), spatially inhomogeneous perturbations of the form $(\delta A, \delta B) = (\Phi_A, \Phi_B) e^{\alpha t + i\mathbf{q} \cdot \mathbf{r}}$, where the perturbations have a growth rate α , amplitudes (Φ_A, Φ_B) and wave vector $\tilde{\mathbf{q}} = (\tilde{q} \cos \theta, \tilde{q} \sin \theta)$. The wave vector is assumed to make an angle θ with the direction of the flow in the (x, y) plane. The concentration of species A and B can then be written as

$$\tilde{A} = \tilde{A}_e + \Phi_A e^{\alpha t} e^{i\tilde{\mathbf{q}} \cdot \mathbf{r}}, \quad \tilde{B} = \tilde{B}_e + \Phi_B e^{\alpha t} e^{i\tilde{\mathbf{q}} \cdot \mathbf{r}}. \quad (4.2)$$

Inserting this ansatz in the kinetic Eqs.(4.1a) and (4.1b) we obtain

$$\alpha \begin{bmatrix} \Phi_A \\ \Phi_B \end{bmatrix} = \begin{bmatrix} \tau \left(2\eta \tilde{A}_e^\pm \tilde{B}_e^\pm - 1 - \frac{\tilde{q}^2}{\varepsilon^2} - \frac{i\tilde{q}\delta\tilde{u}\cos\theta}{\tau} \right) & \tau\eta\tilde{B}_e^{\pm 2} \\ -2\tilde{A}_e^\pm \tilde{B}_e^\pm & -(\tilde{q}^2 + \tilde{B}_e^{\pm 2} + 1 + i\tilde{q}\tilde{u}\cos\theta) \end{bmatrix} \begin{bmatrix} \Phi_A \\ \Phi_B \end{bmatrix}. \quad (4.3)$$

We consider the non-trivial states $(\tilde{A}_e^\pm, \tilde{B}_e^\pm)$. From Eq. (2.7) the equilibrium states can be written as $\tilde{A}_e^\pm = 1/\eta\tilde{B}_e^\pm$ and $\tilde{B}_e^{\pm 2} + 1 = \eta\tilde{B}_e^\pm$. Substituting these relations in matrix equation (4.3) we arrive at the eigenvalue equation

$$|\mathbf{M} - \alpha\mathbf{I}|\Phi = 0, \quad (4.4)$$

where \mathbf{I} is the unit matrix and the matrix \mathbf{M} in this case is given as:

$$\mathbf{M} = \begin{bmatrix} \tau \left(1 - \frac{\tilde{q}^2}{\varepsilon^2} - \frac{i\tilde{q}\delta\tilde{u}\cos\theta}{\tau} \right) & \tau\eta\tilde{B}_e^\pm \\ -\frac{2}{\eta} & -(\tilde{q}^2 + \eta\tilde{B}_e^\pm + i\tilde{q}\tilde{u}\cos\theta) \end{bmatrix}. \quad (4.5)$$

The trace and determinant of matrix M can be written as

$$\text{tr}M = -\tilde{q}^2 \left(1 + \frac{\tau}{\varepsilon^2}\right) - i\tilde{q}\tilde{u}(1+\delta)\cos\theta + (\tau - \eta\tilde{B}_e^\pm), \quad (4.6a)$$

$$|M| = \frac{\tau\tilde{q}^4}{\varepsilon^2} + i\tilde{q}^3 \left(\frac{\tau\tilde{u}}{\varepsilon^2} + \tilde{u}\right) + \tilde{q}^2 \left(\frac{\tau\eta\tilde{B}_e^\pm}{\varepsilon^2} - \tau - \tilde{u}^2\right) + i\tilde{q}\tilde{u}(\eta\tilde{B}_e^\pm - \tau) + \tau(\eta\tilde{B}_e^\pm - 2). \quad (4.6b)$$

This can be re-written in a more shorthand notation as

$$\text{tr}M = a + ib, \quad |M| = c + id \quad (4.7)$$

where the parameters a, b, c and d are given as

$$a = -\tilde{q}^2 \left(1 + \frac{\tau}{\varepsilon^2}\right) + (\tau - \eta\tilde{B}_e^\pm), \quad b = -\tilde{q}\tilde{u}(1+\delta)\cos\theta, \quad (4.8a)$$

$$c = \frac{\tau\tilde{q}^4}{\varepsilon^2} + \tilde{q}^2 \left(\frac{\tau\eta\tilde{B}_e^\pm}{\varepsilon^2} - \tau - \delta\tilde{u}^2\cos^2\theta\right) + \tau(\eta\tilde{B}_e^\pm - 2), \quad (4.8b)$$

$$d = \tilde{u}\cos\theta(\tilde{q}^3(\tau/\varepsilon^2 + \delta) + \tilde{q}(\delta\eta\tilde{B}_e^\pm - \tau)). \quad (4.8c)$$

The dispersion relation obtained from the solution of Eq. (4.4) is written as:

$$\alpha^2 - \alpha\text{tr}M + |M| = 0. \quad (4.9)$$

The eigenvalues α are the characteristic solution of the polynomial equation (4.9). This can be written in terms of shorthand notation as:

$$\alpha_{1,2} = \frac{1}{2} \left((a + ib) \pm \sqrt{(a^2 - b^2 - 4c) + i(2ab - 4d)} \right). \quad (4.10)$$

Evaluating the complex term in the square root by separating the solution into the real and imaginary part one obtains the eigenvalue solutions as

$$\text{Re}[\alpha] = \frac{a}{2} \pm \frac{1}{2} \sqrt{\frac{r + (a^2 - b^2 - 4c)}{2}}, \quad \text{Im}[\alpha] = \frac{b}{2} \pm \frac{1}{2} \sqrt{\frac{r - (a^2 - b^2 - 4c)}{2}}, \quad (4.11)$$

where $r = \sqrt{(a^2 - b^2 - 4c)^2 + (2ab - 4d)^2}$.

Instability in the system sets in when $\text{Re}[\alpha(\tilde{q})] > 0$ for some wave numbers \tilde{q} . The type of instability depends on whether this occurs for $\tilde{q} = 0$ (Hopf instability) or for $\tilde{q} \neq 0$ (corresponding to a Turing instability if, in addition, $\text{Im}[\alpha(\tilde{q})] = 0$). In this work, we focus only on the effect of advection by a uniform flow on the Turing instability. In the absence of flow, the Turing instability in this system sets in when $\varepsilon > \eta\tilde{B}_e^\pm$. In the following, we restrict the discussion to two cases of uniform advection, associated with two values of the parameter δ in Eq. (2.3). First, we consider the trivial – but for test purposes still interesting – case of $\delta = 1$, i.e., the advection of all concentration fields with the flow. Due to Galilean invariance, we expect here a trivial transport of existing patterns with the flow

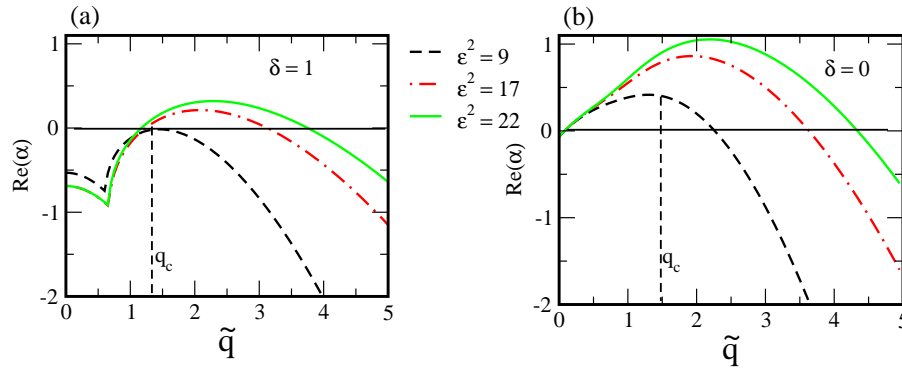


Figure 1: Dispersion relations showing the effect of advection on the real part of the growth rate. (a) $\delta = 1.0$, ($\tau > \eta B_e^\pm$); (b) $\delta = 0$, ($\tau > \eta B_e^\pm$). The graph shows the interaction between Turing instability and differential flow induced instability.

without any modification of the stability phase diagram. In the second, less trivial case of $\delta = 0$, only the concentration field A is advected with the flow (differential advection).

Case I ($\delta = 0$): In this case, species A and B are advected differentially and the real part of the growth rate $\text{Re}[\alpha(\tilde{q})]$ depends on the magnitude and orientation of the advective velocity \tilde{u} . Therefore, the instability is influenced by the flow. An important feature of differential advection is shown by comparing Fig. 1 (a) and (b). In Fig. 1 (a), the growth rate corresponding to $\varepsilon^2 = 9$ is negative for all wave vectors \tilde{q} , meaning that the equilibrium state is stable with respect to any infinitesimal spatially inhomogeneous perturbation. However, in the presence of differential advection, ($\delta = 1$), the growth rate becomes positive for a range of \tilde{q} values, meaning that differential advection can induce instability even if the condition for Turing instability is not fulfilled. Note that, the patterns obtained under this condition are not Turing patterns but are known as differential flow induced patterns. Apart from the differential advection parameter δ , the magnitude and orientation of the advective velocity plays an important role in the range of unstable wave numbers. By increasing the magnitude of the advective velocity, for a constant differential advection parameter δ , the real part of the growth rate takes up more positive values and the maximum is shifted to the long-wavelength limit. In other words, the fastest growing mode and the final selected length scale depend on the advective velocity. Assuming that $(a^2 - b^2 - 4c) \gg (2ab - 4d)$, a simple relation between the fastest growing mode q_c and the imposed velocity u can be derived from Eq. (4.11) by setting $\text{Re}[\alpha] = 0$. One thus obtains:

$$q_c^2 \approx \frac{\varepsilon^2(2 - 1/\tau(1 - \delta)^2 u^2 \cos^2 \theta) - 2\eta B_e^-}{2l_A^2}. \tag{4.12}$$

Case II ($\delta = 1$): The expression for the growth rates in Eq. (4.11) shows that, in the case of $\delta = 1$, as expected, $\text{Re}[\alpha(\tilde{q})]$ is independent of the advection velocity and the onset of the Turing instability is unaffected by the flow. This means that the linearly unstable

modes are the same as that in the absence of the flow. This fact is confirmed by our numerical simulation as shown in the following discussions. The fastest growing mode \tilde{q}_c or the mode with the maximum linear growth rate α can be obtained from Eq. (4.11) by differentiating α with respect to \tilde{q}^2 . In this case, this is written as:

$$\tilde{q}_c^2 = \frac{1}{l_A^2} \frac{\varepsilon^2 - \eta \tilde{B}_e^-}{2}. \quad (4.13)$$

As expected, the wave length of the patterns is also independent of the velocity. The imaginary part of α for $\delta = 1$ obtained from Eq. (4.11) is given as $\text{Im}[\alpha] = -\tilde{q}\tilde{u}\cos\theta$. This means that the unstable modes moves with the imposed velocity \tilde{u} . Thus, in a constant uniform velocity field \tilde{u} the result is just a translational motion of the original Turing patterns.

4.2 Numerical simulation

In this section, we perform numerical simulation of the model equations using the above described LB approach. In order to isolate the effects due to boundary conditions and flow velocity, we start with the situation corresponding to no fluid flow ($\mathbf{u} = 0$) and performed simulations for various values of the parameter η on a domain with periodic boundary condition (PBC) in all directions (upper row in Fig. 2) and a domain with PBC along the x -direction and no-flux boundary condition at the top and bottom (lower row in Fig. 2).

Using the patterns obtained in the absence of flow as initial conditions, we impose a uniform flow in a channel of dimension 100×400 (l.u.) with periodic boundary condition (PBC) in all directions.

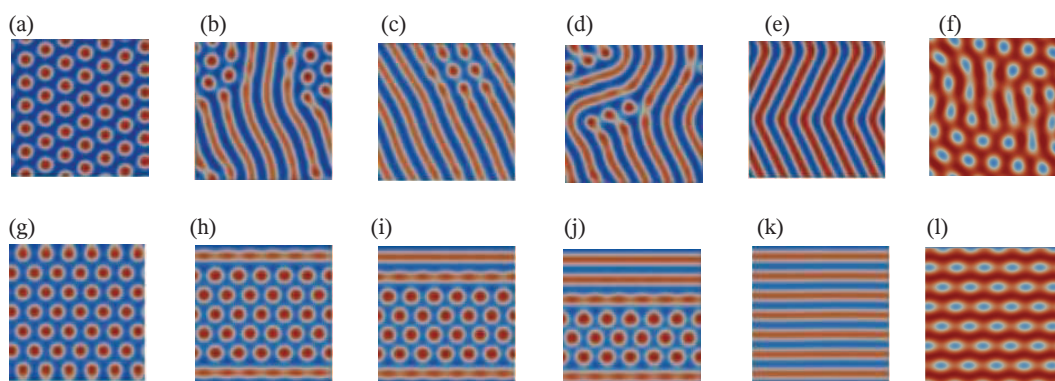


Figure 2: Patterns obtained in the absence of advective flow fields. The upper row shows solutions with periodic boundary conditions and the lower row depicts solutions with no-flux wall boundary condition. The values of η from left to right are: 2.1052, 2.1988, 2.2388, 2.2531, 2.2798, 2.4530. In all the cases investigated here, we take $\tau = 2.744$ and $\varepsilon = 4.62$.

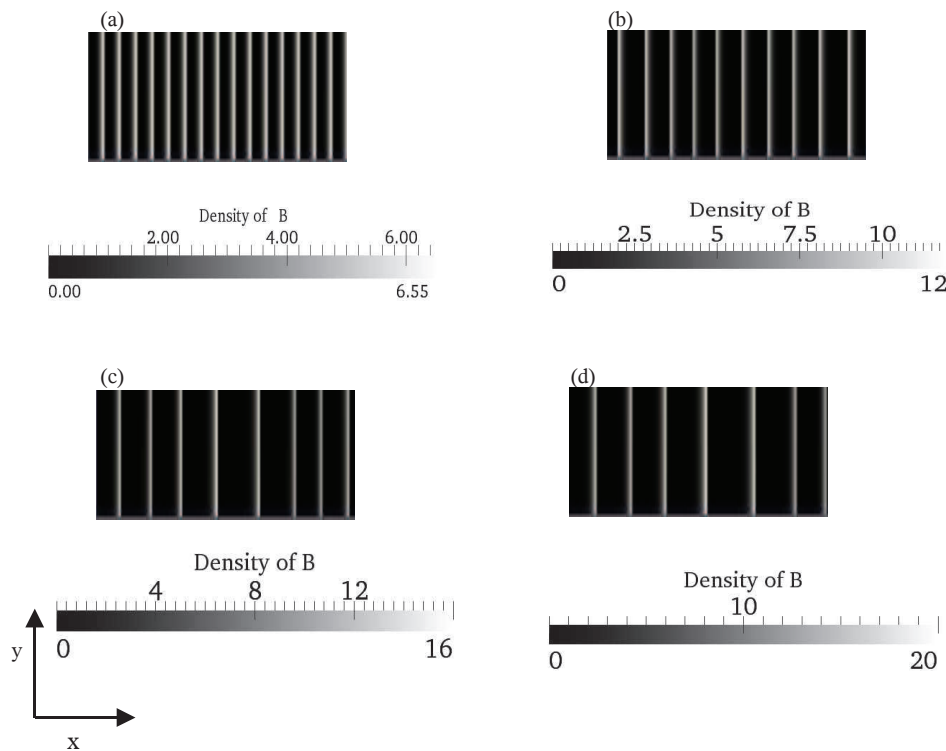


Figure 3: Patterns obtained under a constant uniform flow in the x -direction with differential advection parameter $\delta=0$ (species B is immobile). (a) $u=0.01$; (b) $u=0.03$; (c) $u=0.05$; (d) $u=0.07$. The patterns consist of traveling stripes along the flow direction.

We first consider the case $\delta=0$. In this case, species A is advected and spatially disengaged from species B, thus allowing B to grow locally. In this case, the general solution consists of traveling stripes with wave vector parallel with the flow direction ($\theta=0^0$). The snapshots of the solutions taken in the frame of reference moving at a constant velocity u along the x -direction are shown in Fig. 3. Note that the transition to the traveling stripe structure is not sharp but rather smooth. It takes time of order $t > l_x/u$ in order to have a fully developed structure from the initial Turing structure in Fig. 2a to the final traveling stripe structures in Fig. 3. As predicted by the linear stability analysis in Eq. (4.12), the wave length of these stripes is found to vary with the magnitude of the flow velocity. In addition to this, note the gradual increase in the density of species B with increasing velocity, this results from the tendency of species B to grow more locally as species A is being advected faster away. This observation is interesting and has a close similarity to vegetative pattern formation along sloppy hill side, where plant growths depends on sufficient water run-off downhill [39]. Fig. 3a-d show the solutions obtained by varying the magnitude of the flow velocity in the x -direction from 0.01 to 0.07. The computed wave length of the patterns shown in Fig. 3 are found to be close to the predictions of

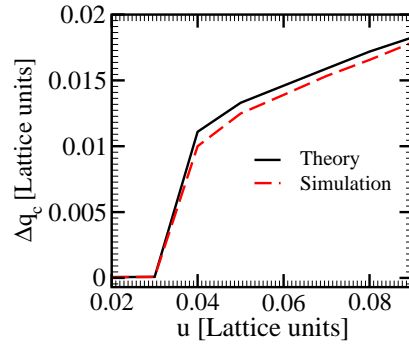


Figure 4: Plot of change in the maximum growth mode Δq_c with velocity increase in steps of 0.01. The solid line is the theory computed from Eq. (4.12) by setting $\tau = 2.744$, $\eta = 2.1988$ and $\varepsilon^2 = 22.61$. The dashed line is the simulation data obtained with the same values of parameters.

Eq. (4.12). We made a comparison of the theory and simulation in Fig. 4 by plotting the change in the fastest growth mode $\Delta q_c = q_c(u_i) - q_c(u_f)$ as the velocity is increased in steps of 0.01 where u_i is the velocity at the initial step and u_f is the velocity at the final step. The theoretical data are calculated from Eq. (4.12) using the parameter values $\tau = 2.744$, $\eta = 2.1988$ and $\varepsilon^2 = 22.61$. The simulation data are obtained by computing the wavevector of the patterns in Fig. 3 using the relation $q = 2\pi n_x / L_x$, where n_x is the wave number and L_x is lattice dimension along the x -axis. The simulation and theory are found to agree within about 5% error in the worst case. As a further verification of the above results, we look at situations where the velocity field of magnitude $|u|$ is oriented at an angle ψ to the x -axis. Fig. 5 shows the results obtained for different values of the angle ψ and velocity $|u|$ of the flow field. It is interesting to observe that under this condition the stripes are also perpendicular to the flow direction or in other words the wave vector is parallel to the flow direction. This is in line with a study of the angle dependence of the growth rate, which reveals that the fastest growing mode corresponds to $\theta = 0^\circ$.

For $\delta = 1$, corresponding to the absence of differential advection, both species are advected equally with the same velocity. Under a constant uniform flow, the solution is spatial translation of the original Turing pattern in Fig. 2. However, under Poiseuille flow, the non-uniformity of the velocity field along the y -direction may break the symmetry and the solution may bifurcate into Turing structures with stripes aligned along the streamlines and wave vector perpendicular to the flow direction (not shown). A detailed discussion of this issue will be presented elsewhere.

In summary, we present a LB model for simulating pattern formation in ADR equations. We found that pattern formation under a uniform flow with differential advection mechanism, leads to traveling stripes with a velocity dependent wave vector parallel to the flow direction. This holds regardless of the flow direction with respect to the lattice orientation, thus underlining the physical relevance of the observation. These observations from the Lattice Boltzmann simulations of the ADR equations are shown to be in line with the theoretical predictions from linear stability analysis.

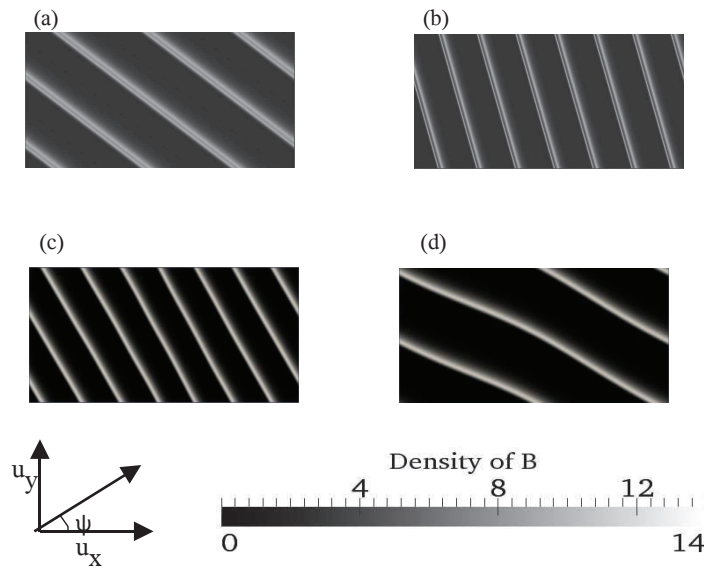


Figure 5: Patterns obtained under a constant uniform flow with the velocity magnitude $|u|$ at an angle ψ with the x -direction. (a) $|u| = 0.05$, $\psi = 36.89^\circ$; (b) $|u| = 0.05$, $\psi = 53.13^\circ$; (c) $|u| = 0.02$, $\psi = 45^\circ$; (d) $|u| = 0.044$, $\psi = 26.56^\circ$.

Acknowledgments

This work was supported by the Max-Planck-Institut für Eisenforschung and by the Interdisciplinary Centre for Advanced Material Simulation (ICAMS), Ruhr Universität Bochum.

References

- [1] F. T. Arecchi, S. Boccaletti, and P. Ramazza, *Phys. Rep.*, 318, 1, (1999).
- [2] R. E. Wilson, *Phil. Trans. R. Soc. A*, 366, 2017 (2008).
- [3] I. R. Epstein and K. Showalter, *J. Phys. Chem.*, 100, 13132 (1996).
- [4] A. De Wit, *Adv. Chem. Phys.*, 109, 435 (1999).
- [5] F. Sagu and I. R. Epstein, *Dalton Trans.*, 1201 (2003).
- [6] J. D. Murray, *Mathematical Biology: I. An Introduction* (2002).
- [7] J. D. Murray, *Mathematical Biology: II. Spatial Models and Biomedical Applications*, (2003).
- [8] I. R. Epstein, *Proc. Nat. Acad. Sci.*, 103, 15727 (2006).
- [9] S. Kitsunzaki, *Physica D*, 216, 294 (2006).
- [10] A. A. Polezhaev, R.A. Pashkov, A.I. Lobanov, and I.B. Petrov, *Int.J.Dev.Biol.*, 50, 309 (2006).
- [11] S. J. Schiff, X. Huang, and J.-Y Wu, *Phys. Rev. Lett.* 98, 178102 (2007).
- [12] A.M. Turing, *The chemical basis of morphogenesis*, *Philos. Trans. R. Soc.*, 237 (1952).
- [13] G. Nicolis and I. Prigogine, *Self-Organization in Nonequilibrium Systems: from Dissipative Structures to Order through Fluctuations*, Wiley, New York (1977).
- [14] J. Tabony, N. Glade, J. Demongeot and C. Papaseit, *Langmuir*, 18, 7196 (2002).

- [15] P. Andresen, M. Bache, E. Mosekilde, G. Dewel, and P. Borckmanns, *Phys. Rev. E* 60, 297 (1999).
- [16] M. Kærn and M. Menzinger, *Phys. Rev. E* 60, R3471 (1999).
- [17] M. Kærn, M. Menzinger, and A. Hunding, *J. Theor. Biol.* 207, 473 (2000).
- [18] M. Kærn, M. Menzinger, R. Satnoianu, and A. Hunding, *Faraday Discuss.* 120, 295 (2002).
- [19] P.W. Boyd et al., *Nature* 407, 695 (2000).
- [20] A.P. Martin, *Prog. Oceanography* 57, 125 (2003).
- [21] P.A. Bachmann, P.L. Luisi, and J. Lang, *Nature*, 357, 57 (1992).
- [22] M. A. Bedau, J. S. McCaskill, N. H. Packard, S. Rasmussen, C. Adami, D. G. Green, *Artificial Life*, 6, 363 (2000).
- [23] J.E. Pearson, *Science* 261, 189 (1993).
- [24] E.G. Flekkoy, *Phys. Rev. E* 47, 4247 (1993).
- [25] A. Xu, G. Gonnella, and A. Lamura *Phys. Rev. E* 67, 056105 (2003).
- [26] S. G. Ayodele, F. Varnik, and D. Raabe, *Phys. Rev. E* 83, 016702 (2011).
- [27] G. R. McNamara and G. Zanetti, *Phys. Rev. Lett.* 61, 2332 (1988).
- [28] F. Higuera, S. Succi, and R. Benzi, *Europhys. Lett.* 9, 345 (1989).
- [29] Y. Qian, D. d'Humieres, and P. Lallemand, *Europhys. Lett.* 17, 479 (1992).
- [30] S. Succi, *The Lattice Boltzmann Equation: for Fluid Dynamics and Beyond*, Oxford University Press, (2001).
- [31] R. Rubinstein, and L.S. Luo, *Phys. Rev. E* 77, 036709 (2008).
- [32] S. Arcidiacono, I. V. Karlin, J. Mantzaras, and C. E. Frouzakis, *Phys. Rev. E* 76, 046703 (2007).
- [33] S. Arcidiacono, J. Mantzaras, and I. V. Karlin, *Phys. Rev. E* 78, 046711 (2008).
- [34] S. Chapman and T. G. Cowling, "The Mathematical Theory of Non-uniform Gases," 3rd ed., Cambridge University press, Cambridge (1970).
- [35] D. A. Wolf-Gladrow, "Lattice-Gas Cellular Automata and lattice Boltzmann Models", *Lecture Notes in Mathematics* 1725, Springer-Verlag, Berlin/Heidelberg (2000).
- [36] B. Chopard, J.L. Falcone, and J. Latt, *Eur. Phys. J. Special Topics* 171, 245 (2009).
- [37] H.-B Huang, X.-Y Lu and M. C. Sukop, *J. Phys. A: Math. Theor.* 44, 055001 (2011).
- [38] M. Beck, A. Ghazaryan and B. Sandstede. *J. Differential Equations* 246, 4371 (2009).
- [39] J. A. Sherratt, *Proc. R. Soc. A*, 467, 3272 (2011).